

Note: This paper has been published in [Physical Chemistry Chemical Physics](https://doi.org/10.1039/C5CP03102H), which can be viewed at the following URL:
<http://doi.org/10.1039/C5CP03102H>

Intrinsic defects in photovoltaic perovskite variant Cs_2SnI_6

Zewen Xiao,^{1,2} Yuanyuan Zhou,³ Hideo Hosono,^{1,2} Toshio Kamiya^{1,2}

¹Materials and Structures Laboratory, Tokyo Institute of Technology, Yokohama 226-8503, Japan

²Materials Research Center for Element Strategy, Tokyo Institute of Technology, Yokohama 226-8503, Japan

³School of Engineering, Brown University, Providence, RI 02912, United States

ABSTRACT: Cs_2SnI_6 is a variant of perovskite materials and is expected as a lead-free air-stable photovoltaic material. In this letter, we report intrinsic defects in Cs_2SnI_6 using first-principles density functional theory calculations. It is revealed that iodine vacancy and tin interstitial are the dominant defects that are responsible for the intrinsic n -type conduction in Cs_2SnI_6 . Tin vacancy has a very high formation energy (>3.6 eV) due to the strong covalency in the Sn–I bonds and is hardly generated for p -type doping. All the dominant defects in Cs_2SnI_6 have deep transition levels in the band gap. It is suggested that the formation of the deep defects can be suppressed significantly by employing an I-rich synthesis condition, which is inevitable for photovoltaic and other semiconductor applications.

Metal halide perovskites have been introduced as the “game-changer” materials in the novel solid-state solar cells.^{1–4} These perovskite compounds have the general chemical formula ABX_3 ($A = \text{Cs}$, CH_3NH_3 , or $\text{CH}_2\text{NH}=\text{CH}$; $B = \text{Pb}$ or Sn ; $X = \text{I}$, Br or Cl), where the A cations sit in the cubic or pseudo-cubic network of corner-sharing BX_6 octahedra (see Fig. 1a). Among these materials, tin (Sn) based perovskites ASnX_3 have attracted particular interest due to their nontoxicity.^{5–9} However, ASnX_3 are very sensitive to the ambient atmosphere (oxygen, moisture, etc.)^{7–12} and exploration for air-stable alternatives has become an urgent issue. Promisingly, Lee *et al.*¹³ recently reported that the Sn-based perovskite variant Cs_2SnI_6 exhibited high air-stability and their solar cells exhibit good efficiency as high as 8%. It is proposed that the superior stability of Cs_2SnI_6 to CsSnI_3 would be attributed to the +4 oxidation state of Sn in Cs_2SnI_6 based on a simple ionic model;¹³ on the other hand, density functional / hybrid density functional theory (DFT/HDFT) calculations indicate that the real oxidation state of Sn in Cs_2SnI_6 is closer to +2, similar to CsSnI_3 , which originates from the nominal formula $\text{Cs}^+_2\text{Sn}^{2+}\text{I}_6^{4-}$.¹⁴ In this view, the improved stability of Cs_2SnI_6 is attributed to the strong covalency of the Sn–I bonds in the isolated $[\text{SnI}_6]^{2-}$ cluster.

It is known well that the typical Sn^{2+} -based compounds, including SnO ,¹⁵ SnS ,¹⁶ and CsSnI_3 ,¹⁷ in general, intrinsically exhibit good p -type conductivity because V_{Sn} in these compounds are easily formed and act as shallow acceptors to produce mobile holes. On the other hand, Cs_2SnI_6 have not shown p -type conductivity unlike the other Sn^{2+} -based compounds and have shown n -type conduction or insulating behavior depending on the synthetic routes. Lee *et al.*¹³ reported the native n -type conduction with electron density (n) of $\sim 1 \times 10^{14} \text{ cm}^{-3}$ in polycrystalline Cs_2SnI_6

pellets annealed at 200 °C, while Zhang *et al.*¹⁸ observed very high resistivity in room temperature-processed Cs_2SnI_6 . Therefore, in order to clarify the intrinsic nature of Cs_2SnI_6 and its origin, a systematic theoretical study on the intrinsic defects is important, which will provide a guiding principle for tuning its properties for photovoltaic and other semiconductor applications.

Here, we studied the formation enthalpy (ΔH) of intrinsic defects in Cs_2SnI_6 by DFT/HDFT calculations. It was clarified that I vacancy (V_{I}) and Sn interstitial (Sn_{i}) are mainly responsible for the intrinsic n -type conductivity in Cs_2SnI_6 . V_{Sn} , which is usually a dominant p -type defect in Sn^{2+} -based compounds, is hardly formed in Cs_2SnI_6 because of its high ΔH which is caused by the strong covalency of the Sn–I bonds in the isolated $[\text{SnI}_6]^{2-}$ cluster. It was also clarified that intrinsic p -type conductivity is hardly attained in pure Cs_2SnI_6 due to the absence of an effective acceptor with sufficiently low ΔH and a shallow transition level. The origin of deep transition levels of the dominant defects in Cs_2SnI_6 will be discussed.

Cs_2SnI_6 crystallizes into the anti-fluorite structure (space group $Fm\bar{3}m$, the lattice parameter $a = 11.65 \text{ \AA}$),¹⁹ which is composed of four $[\text{SnI}_6]^{2-}$ octahedra at the corners and the face centers and eight Cs^+ cations at the tetragonal interstitials, as shown in Fig. 1b. Alternatively, Cs_2SnI_6 can be regarded as a defective variant of the simple perovskite CsSnI_3 as seen by comparing Figs. 1b with 1a, which illustrates a $2 \times 2 \times 2$ supercell of CsSnI_3 where the $[\text{SnI}_6]^{2-}$ octahedra connect to each other by sharing their corners. The Cs_2SnI_6 structure is obtained by removing a half of the Sn atoms at each center of the $[\text{SnI}_6]$ octahedron at intervals (i.e. those at the centers of orange octahedra in Fig. 1a) and relaxing the resulted structure, and thus the corner-shared $[\text{SnI}_6]^{2-}$ octahedra in Fig. 1a become isolated in Cs_2SnI_6 (Fig. 1b). It should be noted that the $[\text{SnI}_6]^{2-}$ octahedra shrink in the structural relaxation, leading to the smaller Sn–I bond length (2.85 Å)¹⁹ in Cs_2SnI_6 than that in CsSnI_3 (3.11 Å).⁹

Defect calculations were performed for Cs_2SnI_6 in the framework of DFT/HDFT using the projector-augmented wave (PAW) method as implemented in the VASP code²⁰ (see the ESI† for details). Fig. 1c shows the calculated chemical potential ($\Delta\mu_{\text{Sn}}$, $\Delta\mu_{\text{I}}$) – phase map, in which the yellow region A–B–C–D indicates where Cs_2SnI_6 is stabilized against possible competitive phases including Cs, Sn, I, CsI, SnI_2 , SnI_4 , and CsSnI_3 . The narrow shape indicates that the growth conditions should be carefully controlled to produce the single-phase Cs_2SnI_6 , similar to the cases of CsSnI_3 ¹⁷ and MAPbI_3 .²¹

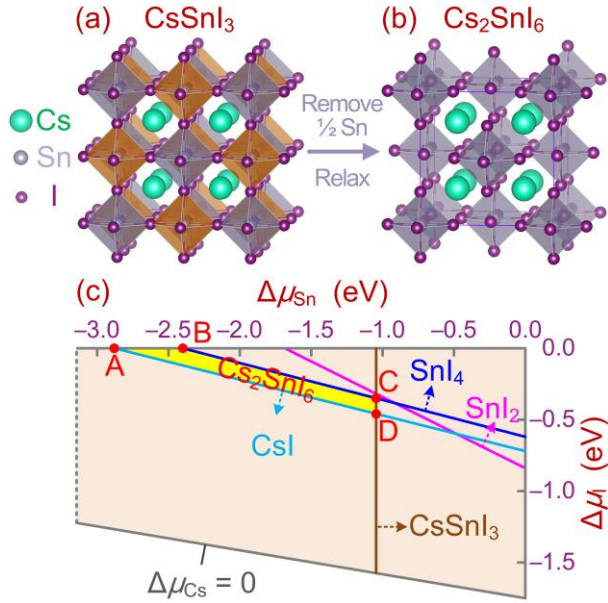


Fig. 1. (a) $2 \times 2 \times 2$ supercell structure of Cs_2SnI_6 . (b) Crystal structure of Cs_2SnI_6 (cubic, space group $Fm\bar{3}m$, $a = 11.65 \text{ \AA}$) where Cs, Sn, and I atoms lie at the $8c$ ($1/4, 1/4, 1/4$), $4a$ ($0, 0, 0$) and $24e$ ($0.245, 0, 0$) sites, respectively. (c) Chemical potential ($\Delta\mu_{\text{Sn}}$, $\Delta\mu_{\text{I}}$) – phase map. The yellow region A–B–C–D shows the region where Cs_2SnI_6 is stabilized against possible competitive phases including Cs, Sn, I, CsI, SnI_2 , SnI_4 , and CsSnI_3 .

We have considered intrinsic point defects in Cs_2SnI_6 including three vacancies (V_{Cs} , V_{Sn} , V_{I}), three interstitials (Cs_i , Sn_i , I_i), two cation substitutions (Cs_{Sn} , Sn_{Cs}), and four antisites (Cs_i , Sn_i , I_{Cs} , I_{Sn}). Two representative chemical potential conditions in Fig. 1c are chosen for the following discussion; ($\Delta\mu_{\text{Cs}}$, $\Delta\mu_{\text{I}}$) at A (I-rich condition) and D (I-poor condition) points, where the calculated ΔH under are plotted as a function of the Fermi level (E_{F}) in Figs. 2a and 2b, respectively. The calculated transition levels $\varepsilon(q/q')$ are plotted relative to the conduction band minimum (CBM) and valence band maximum (VBM) in Fig. 3. Out of the twelve intrinsic defects, four (V_{I} , Sn_i , Cs_i and V_{Cs}) have a sufficiently small ΔH (e.g., $< 1.0 \text{ eV}$) to influence the electrical properties. Among them, V_{I} has the lowest ΔH ($\leq 0.74 \text{ eV}$ and $\leq 0.28 \text{ eV}$ under the I-rich and I-poor conditions, respectively) and acts as a deep donor with $\varepsilon(0/+1) = 0.74 \text{ eV}$ above VBM (i.e., 0.52 eV below the conduction band edge, CBM), which is mainly responsible for the n -type condition of Cs_2SnI_6 . Under the I-poor condition, Sn_i has a small ΔH ($\leq 1.18 \text{ eV}$) and a shallower transition $\varepsilon(0/+1)$ at 0.11 eV below the CBM. Therefore, Sn_i as well as V_{I} are also dominant donors for n -type conduction. Cs_i is of a low ΔH but stabilized in neutral charge state at high E_{F} (i.e. n -type conditions); therefore, it does not contribute to the n -type conduction. Only Sn_i is a shallow donor in Cs_2SnI_6 with the $\varepsilon(0/+2)$ above the CBM, as seen in Figs. 2b and 3. However, because of its high ΔH , Sn_i has limited contribution to the n -type conductivity even under the I-poor condition. On the other hand, under the I-rich condition, V_{Cs} has a low ΔH ($\leq 1.37 \text{ eV}$) and can act as a deep acceptor, but at E_{F} only above 0.51 eV from the VBM and the hole density produced is too low to compensate the electrons released by V_{I} .

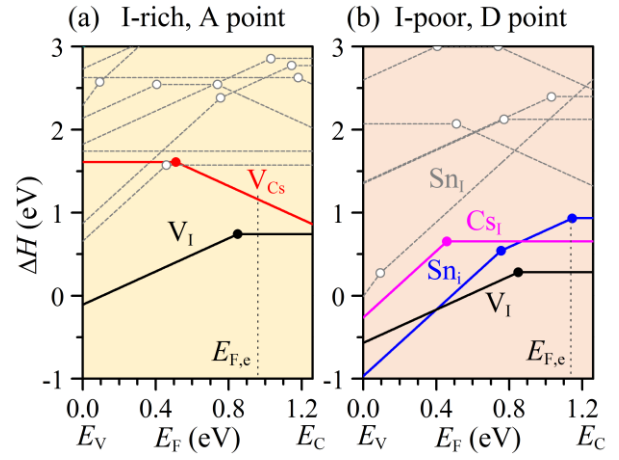


Fig. 2. Calculated ΔH of intrinsic defects in Cs_2SnI_6 as a function of E_{F} at the chemical potential points in Fig. 1c, (a) A (I-rich) and (b) D (I-poor). Defects with much high ΔH values are shown by dashed lines.

The other intrinsic defects with prohibitively high ΔH are displayed by gray dashed lines in Fig. 2. It should be noted that V_{Sn} in Cs_2SnI_6 has high ΔH values under all the chemical potentials and is as large as 3.63 eV even under the Sn-poor condition (A point), as seen in Table 1. This is strikingly different from the cases of the typical Sn^{2+} -based semiconductors such as SnO , SnS , and CsSnI_3 , in which the ΔH values of V_{Sn} (at the VBM) are usually very small under the Sn-poor condition (i.e., 1.3 eV at E_{V} for SnO ,¹⁵ 0.8 eV for SnS ,¹⁶ and 0.3 eV for CsSnI_3 ¹⁷). As we previously reported, the Sn–I bonds in Cs_2SnI_6 exhibit a strong covalency (2.40 eV/bond) due to the much shortened Sn–I length in the isolated $[\text{SnI}_6]^{2-}$ octahedra.¹⁴ Sn atoms are tightly encased in the $[\text{I}_6]$ octahedra and hardly removed by thermal fluctuation, which explains the unusually high ΔH of V_{Sn} in Cs_2SnI_6 . Due to the same reason, the substitutions of Sn by Cs and I (i.e., Cs_{Sn} and I_{Sn}) have similarly high ΔH values. We have proposed that the +2 valence state of Sn in Cs_2SnI_6 is stabilized by the strong covalency of the Sn–I bonds.¹⁴ Here, the high ΔH of the Sn-site-related defects further support the stabilized +2 valence state of Sn in Cs_2SnI_6 .

Since it is found any intrinsic defect does not work as an effective p -type source from the I-rich to I-poor conditions, as shown above, it would be difficult to achieve intrinsic p -type conduction in pure Cs_2SnI_6 . Instead, Cs_2SnI_6 intrinsically exhibits n -type conduction due to the easy formation of V_{I} and Sn_i donors. For quantitative analysis, the equilibrium E_{F} ($E_{\text{F,e}}$) at room temperature were calculated by solving semiconductor statistic equations self-consistently so as to satisfy the charge neutrality condition (see the ESI† for details). Under the I-rich limit at the A point, $E_{\text{F,e}}$ is 0.96 eV above the VBM (see the vertical dotted line in Fig. 2a) and the corresponding electron density (n) is $\sim 10^{12} \text{ cm}^{-3}$, which is not easily determined by a Hall effect measurement. Under the I-poor condition at the D point, $E_{\text{F,e}}$ is 1.14 eV above the VBM (see the vertical dotted line in Fig. 2b) and n is $\sim 10^{16} \text{ cm}^{-3}$. These theoretical results seem to explain the experimental results reported to date; i.e., the electrical properties of Cs_2SnI_6 ranging from insulating¹⁸ to low-density n -type conduction ($n \sim 1 \times 10^{14} \text{ cm}^{-3}$).¹³

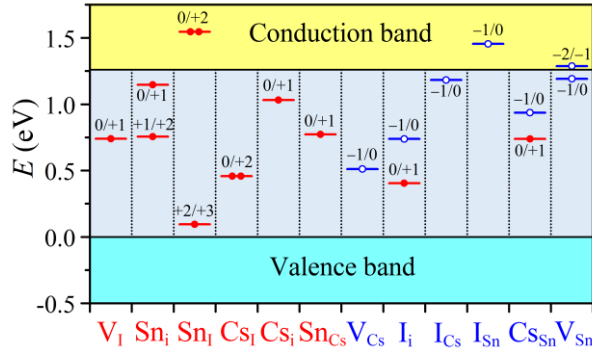


Fig. 3. Calculated transition energy levels $\varepsilon(q/q')$ for intrinsic defects in Cs_2SnI_6 . Donor and acceptor defect levels are denoted by red and blue bars, respectively. The solid and open circles at the transition levels show the number of electrons and holes that can be released during the transition of the defect charge state.

Table 1. Formation enthalpies (in eV) of twelve intrinsic defects in Cs_2SnI_6 at the chemical potential points A, B, C, and D shown in Figure 1.

	V_{Cs}	V_{Sn}	V_{I}	Cs_i	Sn_i	I_i	Cs_{Sn}	Sn_{Cs}	Cs_i	Sn_i	I_{Cs}	I_{Sn}
A	1.61	3.63	0.74	2.86	2.77	2.54	3.74	3.50	1.57	5.47	2.62	1.74
B	1.37	4.11	0.74	3.10	2.28	2.54	4.46	2.78	1.81	4.98	2.38	2.23
C	1.71	5.47	0.40	2.76	0.93	2.88	5.48	1.76	1.14	3.29	3.06	3.92
D	2.07	5.47	0.28	2.40	0.93	3.00	5.12	2.12	0.65	3.17	3.54	4.04

The $\varepsilon(q/q')$ of the dominant defects are important in particular for solar cells because $\varepsilon(q/q')$ in the band gap indicates that they work as an electron trap, hole trap, and/or a recombination center, which deteriorate the device performances. The dominant defects V_{Pb} in MAPbI_3 ²¹ and V_{Sn} in CsSnI_3 ¹⁷ have transition levels deeper than their VBMs and are inert. Also in CuInSe_2 , the dominant defect V_{Cu} has an $\varepsilon(-1/0)$ at only 0.03 eV above the VBM.²² The very shallow V_{Cu} results in good *p*-type good conduction but does not deteriorate the photovoltaic performance. In contrast, in Cs_2SnI_6 , all the dominant defects (Cs_i , Sn_i , V_{I} , V_{Cs} as shown by the solid lines in Fig. 2) have $\varepsilon(q/q')$ in the band gap, as seen in Fig. 3, which would more or less hinder photovoltaic performances through short diffusion/drift length and fast recombination of photo-generated carriers, in particular when processed under the *I*-poor condition. These deep defects can, however, be significantly avoided by using *I*-rich conditions, which is located at the phase boundary between Cs_2SnI_6 and elemental *I* (e.g. the A point as shown in Fig. 2a), because their ΔH are considerably increased as seen in Table 1.

The defect properties as well as electronic structure of a material can qualitatively understood well based on the molecular orbital theory.^{21,23,24} Here we provides a simplified interpretation for the origin of the deep nature of the intrinsic defects in Cs_2SnI_6 in comparison with representative Sn^{2+} -based compounds such as SnO and CsSnI_3 , by focusing on cation and anion vacancies, which generally have low ΔH and play important role on electrical properties of these compounds. Figure 4a shows the calculated densities of states (DOSs) and projected DOSs (PDOSs) for SnO , CsSnI_3 and Cs_2SnI_6 , where the energy is aligned by $\text{Sn } 4d$ and $\text{Cs } 5s$ so as to compare the energy levels. Figures 4b–4d show the schematic energy diagrams that are derived from Fig. 4a. As depicted in Figure 4b, the VBM of SnO consists of the antibonding states of $\text{Sn } 5s$ and $\text{O } 2p$ orbitals (region I in the top panel of Fig. 4a). For a cation vacancy V_{M} , it is known that the V_{M} transition energy in a simple oxide is ~ 1 eV above VBM e.g. in ZnO .²⁵ Also for the SnO case, the V_{Sn} level is above the $\text{O } 2p$ band (re-

gion II of the top panel of Fig. 4a) similar to the V_{M} in the simple oxides. As the VBM made by $\text{Sn } 5s$ level is similarly high, and consequently the V_{Sn} level in SnO forms the shallow acceptor level. On the other hand, the CBM consists of antibonding $\text{Sn } 5p$ - $\text{O } 2p$ states and is close to the $\text{Sn } 5p$ level due to the ionic character of SnO . For an oxygen vacancy V_{O} , the defect state is composed of the Sn non-bonding state, which drops slightly from the CBM,²³ resulting in the shallow nature of V_{O} . Fig. 2c schematically illustrates the formation of the CBM, VBM, V_{Sn} , and V_{I} in CsSnI_3 . Since the Cs cation does not contribute to the electronic structure around the band gap, the electronic structure of CsSnI_3 is similar to that of SnO if O is replaced with I . As a result, V_{Sn} and V_{I} in CsSnI_3 form a shallow acceptor and a shallow donor, respectively, similar to those in SnO .¹⁷

In contrast, Cs_2SnI_6 has a strikingly different electronic structure (see the bottom panel of Fig. 4a and Ref. 14 for details), which is schematically illustrated in Fig. 4d. Because the removal of the half of Sn atoms and the subsequent isolation of the $[\text{SnI}_6]^{4-}$ octahedra, the energy splitting between the bonding and the antibonding states of $\text{Sn } 5s$ – $\text{I } 5p$ (see regions IV and I, respectively, in the bottom panel of Fig. 4a) become very large, and the $\text{Sn } 5s$ – $\text{I } 5p$ bonding energies are deepened; on the other hand, the $\text{Sn } 5s$ – $\text{I } 5p$ antibonding energies are pushed up and become unoccupied states, forming the CBM of Cs_2SnI_6 . The VBM is composed of the $\text{I } 5p$ – $\text{I } 5p$ antibonding states (region II in the bottom panel of Fig. 4a). It should be noted that the $\text{Sn } 5s$ level in Cs_2SnI_6 is deep similar to SnO and CsSnI_3 and almost fully occupied, indicating the $+2$ oxidation state of Sn . It is seen that the V_{Sn} level in Cs_2SnI_6 is similar to those in SnO and CsSnI_3 , while the VBM level in Cs_2SnI_6 is far below that in CsSnI_3 ; consequently, the V_{Sn} in Cs_2SnI_6 is a deep acceptor even close to the CBM, which explains why Cs_2SnI_6 is not an intrinsic *p*-type semiconductor.

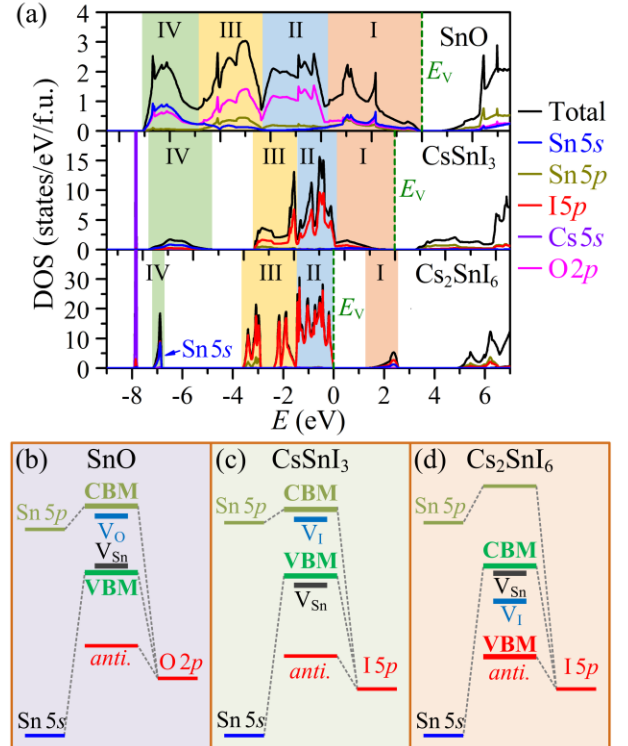


Fig. 4. (a) Total and projected densities of states (DOSs/PDOSs) of $\text{Sn}^{2+}\text{O}^{2-}$ (top panel), $\text{Cs}^+\text{Sn}^{2+}\text{I}_3$ (middle panel), and $\text{Cs}_2^+\text{Sn}^{2+}\text{I}_6^{4-}$ (bottom panel). Simplified energy diagrams depicting the formation of VBM, CBM, and donor-/acceptor-like defects in (b) $\text{Sn}^{2+}\text{O}^{2-}$, (c) $\text{Cs}^+\text{Sn}^{2+}\text{I}_3$, and (d) $\text{Cs}_2^+\text{Sn}^{2+}\text{I}_6^{4-}$.

In summary, we have investigated the formation energies of intrinsic defects in the Cs₂SnI₆ perovskite variant. The dominant defects are donor V_I and Sn_i, giving the calculated electron densities of 10¹²–10¹⁶ cm⁻³. Unlike other Sn²⁺-based *p*-type semiconductor such as SnO, SnS and CsSnI₃, the V_{Sn} in Cs₂SnI₆ has a very high $\Delta H > 3.6$ eV and are hardly formed, primarily because of the strong Sn–I covalent bonds in the functional group-like [SnI₆]²⁻ isolated cluster. The energy levels of the dominant defects are deep in the band gap and would work as recombination centers in photovoltaic applications. On the other hand, their formations would be practically suppressed by employing an I-rich synthesis condition where their densities are negligibly small due to the high ΔH . These results explain the reported experimental results and provide a clue to better understanding the unusual defect physics in *p*-block metal-based compounds.

This work was conducted under Tokodai Institute for Element Strategy (TIES) funded by MEXT Elements Strategy Initiative to Form Core Research Center. Y.Z. thanks Prof. Nitin P. Padture and U.S. National Science Foundation (DMR-1305913) for the support.

REFERENCES

- ¹ M. A. Green and T. Bein, *Nat. Mater.*, 2015, **14**, 559–561.
- ² W. S. Yang, J. H. Noh, N. J. Jeon, Y. C. Kim, S. Ryu, J. Seo and S. I. Seok, *Science*, 2015, **348**, 1234.
- ³ Y. Zhou, M. Yang, W. Wu, A. L. Vasiliev, K. Zhu and N. P. Padture, *J. Mater. Chem. A*, 2015, **3**, 8178.
- ⁴ S. D. Stranks and H. J. Snaith, *Nature Nanotech.*, 2015, **10**, 391–402.
- ⁵ F. Hao, C. C. Stoumpos, D. H. Cao, R. P. H. Chang and M. G. Kanatzidis, *Nat. Photonics*, 2014, **8**, 489.
- ⁶ J. Feng and B. Xiao, *J. Phys. Chem. C*, 2014, **118**, 19655 (2014).
- ⁷ N. K. Noel, S. D. Stranks, A. Abate, C. Wehrenfennig, S. Guarnera, A.-A. Haghighirad, A. Sadhanala, G. E. Eperon, S. K. Pathak, M. B. Johnston, A. Petrozza, L. M. Herz, and H. J. Snaith, *Energy Environ. Sci.* **7**, 3061 (2014).
- ⁸ I. Chung, B. Lee, J. He, R. P. H. Chang, and M. G. Kanatzidis, *Nature* **485**, 486 (2012).
- ⁹ I. Chung, J. H. Song, J. Im, J. Androulakis, C. D. Malliakas, H. Li, A. J. Freeman, J. T. Kenney, and M. G. Kanatzidis, *J. Am. Chem. Soc.* **134**, 8579 (2012).
- ¹⁰ Z. Chen, J. J. Wang, Y. Ren, C. Yu, and K. Shum, *Appl. Phys. Lett.* **101**, 093901 (2012).
- ¹¹ Y. Zhou, H. F. Garces, B. S. Senturk, A. L. Ortiz, and N. P. Padture, *Mater. Lett.* **110**, 127 (2013).
- ¹² E. Lora da Silva, J. M. Skelton, S. C. Parker and A. Walsh, *Phys. Rev. B* **91**, 144107 (2015).
- ¹³ B. Lee, C. C. Stoumpos, N. Zhou, F. Hao, C. Malliakas, C.-Y. Yeh, T. J. Marks, M. G. Kanatzidis, and R. P. H. Chang, *J. Am. Chem. Soc.* **136**, 15379 (2014).
- ¹⁴ Z. Xiao, H. Lei, X. Zhang, Y. Zhou, H. Hosono, and T. Kamiya, *Bull. Chem. Soc. Jpn.* doi:10.1246/bcsj.20150110 (2015).
- ¹⁵ A. Togo, F. Oba, I. Tanaka, and K. Tatsumi, *Phys. Rev. B* **74**, 195128 (2006).
- ¹⁶ Z. Xiao, F.-Y. Ran, H. Hosono, and T. Kamiya, *Appl. Phys. Lett.* **106**, 152103 (2015).
- ¹⁷ P. Xu, S. Chen, H.-J. Xiang, X.-G. Gong, and S.-H. Wei, *Chem. Mater.* **26**, 6068 (2014).
- ¹⁸ J. Zhang, C. Yu, L. Wang, Y. Li, Y. Ren, and K. Shum, *Sci. Rep.* **4**, 6954 (2014).
- ¹⁹ G. Kresse and J. Furthmüller, *Phys. Rev. B* **54**, 11169 (1996).
- ²⁰ W.-J. Yin, T. Shi, and Y. Yan, *Appl. Phys. Lett.* **104**, 063903 (2014).
- ²¹ S. B. Zhang, S.-H. Wei, A. Zunger, and H. Katayama-Yoshida, *Phys. Rev. B* **57**, 9642 (1998).
- ²² W.-J. Yin, S.-H. Wei, M. M. Al-Jassim, and Y. Yan, *Appl. Phys. Lett.* **99**, (2011).
- ²³ W.-J. Yin, T. Shi, and Y. Yan, *J. Phys. Chem. C* **119**, 5253 (2015).
- ²⁴ S. J. Clark, J. Robertson, S. Lany, and A. Zunger, *Phys. Rev. B* **81**, 115311 (2010).